

AD-A179 712

INSTRUMENTATION FOR INFRARED AIRGLOW CLUTTER(U) UTAH
STATE UNIV LOGAN CENTER FOR SPACE ENGINEERING
J C ULMICK 10 MAR 87 CSE/87-012 AFOSR-TR-87-0370

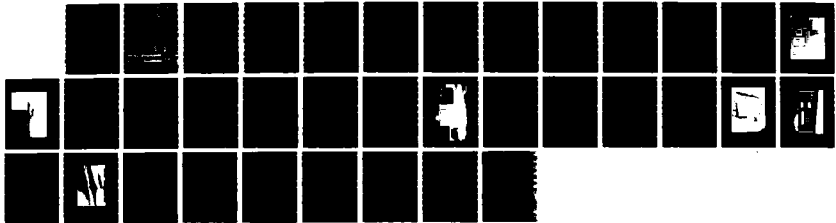
1/1

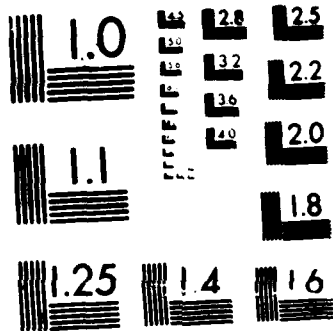
UNCLASSIFIED

AFOSR-84-0192

F/G 4/1

ML





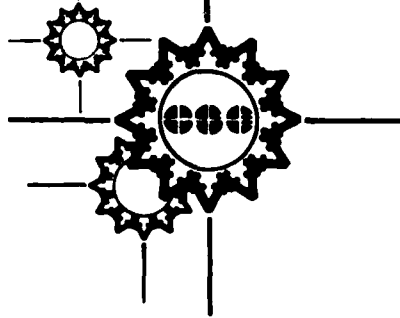
MICROCOPY RESOLUTION TEST CHART
NATIONAL BUREAU OF STANDARDS 1963-A

DTIC FILE COPY

AFOSR-TR- 87-0370

CSE/87-012

AD-A179 712



[Handwritten signature]

MAR 9 1987

**INSTRUMENTATION FOR
INFRARED AIRGLOW CLUTTER**

by
James C. Ulwick

Approved for public release;
distribution unlimited.

10 March 1987

Final Report

Contract AFOSR-84-0192

AIR FORCE OFFICE OF SCIENTIFIC RESEARCH
DIRECTORATE OF CHEMICAL AND ATMOSPHERIC SCIENCE
BOLLING AIR FORCE BASE, WASHINGTON, D.C. 20332-6448
Approved for public release; distribution unlimited.

Prepared for
Air Force Office of Scientific Research
Directorate of Chemical and Atmospheric Science
Bolling AFB, D.C. 20332-6448

DTIC
COLLECTED
APR 27 1987
[Handwritten signature]



CENTER FOR SPACE ENGINEERING
UTAH STATE UNIVERSITY UMC 4140 LOGAN, UTAH 84322

Approved for public release,
distribution unlimited

87 4 00 008

REPORT DOCUMENTATION PAGE

1a. REPORT SECURITY CLASSIFICATION Unclassified		1b. RESTRICTIVE MARKINGS <i>Unclassified</i>	
2a. SECURITY CLASSIFICATION AUTHORITY <i>U</i>		3. DISTRIBUTION/AVAILABILITY OF REPORT <i>Approved for public release, distribution unlimited</i>	
2b. DECLASSIFICATION/DOWNGRADING SCHEDULE			
4. PERFORMING ORGANIZATION REPORT NUMBER(S) CSE/87-012		5. MONITORING ORGANIZATION REPORT NUMBER(S)	
5a. NAME OF PERFORMING ORGANIZATION Center for Space Engineering	5b. OFFICE SYMBOL <i>(If applicable)</i>	7a. NAME OF MONITORING ORGANIZATION Air Force Office of Scientific Research <i>AFOSR/NC</i>	
6c. ADDRESS (City, State and ZIP Code) Utah State University Logan, UT 84322-4140		7b. ADDRESS (City, State and ZIP Code) Directorate of Chemical and Atmos. Research Air Force Office of Scientific Research Bolling AFB, DC 20332-6448	
8a. NAME OF FUNDING/SPONSORING ORGANIZATION AFOSR	8b. OFFICE SYMBOL <i>(If applicable)</i> NC	9. PROCUREMENT INSTRUMENT IDENTIFICATION NUMBER Grant No. AFOSR-84-0192	
6c. ADDRESS (City, State and ZIP Code) Directorate of Chemical and Atmos Science Air Force Office of Scientific Research Bolling AFB, DC 20331-6448		10. SOURCE OF FUNDING NOS.	
11. TITLE (Include Security Classification) Instrumentation for Infrared Airglow (cont)		PROGRAM ELEMENT NO. <i>61102F</i>	TASK NO. <i>2917</i>
12. PERSONAL AUTHOR(S) J.C. Ulwick		PROJECT NO. <i>A2</i>	WORK UNIT NO.
13a. TYPE OF REPORT <i>Final</i>	13b. TIME COVERED FROM <i>7/84</i> TO <i>5/86</i>	14. DATE OF REPORT (Yr., Mo., Day) 10 March 1987	15. PAGE COUNT 31
16. SUPPLEMENTARY NOTATION			
17. COSATI CODES		18. SUBJECT TERMS (Continue on reverse if necessary and identify by block number)	
FIELD	GROUP	SUB. GR.	
		Infrared Emission Measurement, Auroral and Airglow Measurements	
19. ABSTRACT (Continue on reverse if necessary and identify by block number)			
<p>Two measurements systems have been completed to provide the capability to make high resolution spatial and temporal measurements of infrared structures of the aurora & airglow. The two systems are: 1) GAZER (Graphics Aided Zonal Energy Recorder) - a low light level, wide angle TV imaging and recording system with the capability of storing information regarding absolute intensity levels of the image for subsequent recall and analysis; and 2) Scanning IR Radiometer - a microprocessor controlled tracking mount which drives an IR radiometer through programmable repeatable scan patterns to provide sky maps of the temporal and space small and large scale inhomogeneities.</p>			
20. DISTRIBUTION/AVAILABILITY OF ABSTRACT UNCLASSIFIED/UNLIMITED <input type="checkbox"/> SAME AS RPT. <input type="checkbox"/> DTIC USERS <input type="checkbox"/>		21. ABSTRACT SECURITY CLASSIFICATION Unclassified	
22a. NAME OF RESPONSIBLE INDIVIDUAL <i>James P. Koerner, Lt Col USAF</i>		22b. TELEPHONE NUMBER <i>(202) 767-4460</i>	22c. OFFICE SYMBOL <i>NC</i>

REPORT DOCUMENTATION PAGE

1a. REPORT SECURITY CLASSIFICATION Unclassified		1d. RESTRICTIVE MARKINGS Unclassified	
2a. SECURITY CLASSIFICATION AUTHORITY		3. DISTRIBUTION/AVAILABILITY OF REPORT Approved for public release; distribution is unlimited.	
2b. DECLASSIFICATION/DOWNGRADING SCHEDULE		4. PERFORMING ORGANIZATION REPORT NUMBER(S) CSE/87-012	
4. PERFORMING ORGANIZATION REPORT NUMBER(S) CSE/87-012		5. MONITORING ORGANIZATION REPORT NUMBER(S) AFOSR-TR- 87-0370	
6a. NAME OF PERFORMING ORGANIZATION Center for Space Engineering	6b. OFFICE SYMBOL (If applicable)	7a. NAME OF MONITORING ORGANIZATION Air Force Office of Scientific Research AFOSR/NC	
6c. ADDRESS (City, State and ZIP Code) Utah State University Logan, UT 84322-4140		7b. ADDRESS (City, State and ZIP Code) Directorate of Chemical and Atmos. Research Air Force Office of Scientific Research Bolling AFB, DC 20332-6448	
8a. NAME OF FUNDING/SPONSORING ORGANIZATION AFOSR	8b. OFFICE SYMBOL (If applicable) NC	9. PROCUREMENT INSTRUMENT IDENTIFICATION NUMBER Grant No. AFOSR-84-0192	
8c. ADDRESS (City, State and ZIP Code) Directorate of Chemical and Atmos Science Air Force Office of Scientific Research Bolling AFB, DC 20331-6448		10. SOURCE OF FUNDING NOS.	
11. TITLE (Include Security Classification) Instrumentation for Infrared Airglow (cont)		PROGRAM ELEMENT NO. 61102F	PROJECT NO. 2917
12. PERSONAL AUTHOR(S) J.C. Ulwick		TASK NO. A2	WORK UNIT NO.
13a. TYPE OF REPORT Final	13b. TIME COVERED FROM 7/84 TO 5/86	14. DATE OF REPORT (Yr., Mo., Day) 10 March 1987	15. PAGE COUNT 31
16. SUPPLEMENTARY NOTATION			
17. COSATI CODES		18. SUBJECT TERMS (Continue on reverse if necessary and identify by block number)	
FIELD	GROUP	SUB. GR.	
		Infrared Emission Measurement, Auroral and Airglow Measurements	
19. ABSTRACT (Continue on reverse if necessary and identify by block number)			
Two measurements systems have been completed to provide the capability to make high resolution spatial and temporal measurements of infrared structures of the aurora & airglow. The two systems are: 1) GAZER (Graphics Aided Zonal Energy Recorder) - a low light level, wide angle TV imaging and recording system with the capability of storing information regarding absolute intensity levels of the image for subsequent recall and analysis; and 2) Scanning IR Radiometer - a microprocessor controlled tracking mount which drives an IR radiometer through programmable repeatable scan patterns to provide sky maps of the temporal and space small and large scale inhomogeneities.			
20. DISTRIBUTION/AVAILABILITY OF ABSTRACT UNCLASSIFIED/UNLIMITED <input checked="" type="checkbox"/> SAME AS RPT. <input checked="" type="checkbox"/> DTIC USERS <input type="checkbox"/>		21. ABSTRACT SECURITY CLASSIFICATION Unclassified	
22a. NAME OF RESPONSIBLE INDIVIDUAL JAMES P KOERMER, Lt Col, USAF		22b. TELEPHONE NUMBER (Include Area Code) (202) 767-4960	22c. OFFICE SYMBOL NC

11. (Cont'd): Clutter Studies

TABLE OF CONTENTS

	<u>Page</u>
INTRODUCTION	1
APPROACH	2
GAZER	2
Background	2
System Description	3
GAZER Field Operations	13
THE OPTICAL POINTING SYSTEM	17
APPENDIX A	21
Copy of <i>JGR</i> paper by <i>Rees & Luckey</i> "Auroral Electron Energy Derived From Ratio of Spectroscopic Emissions 1. Model Computations"	22

LIST OF FIGURES

<u>Figure No.</u>		<u>Page</u>
1	A conceptual block diagram of the GAZER system	4
2	A block diagram of the GAZER camera head	5
3	A photograph of the GAZER instrument console	6
4	A photograph of the GAZER remote camera controller and the TV camera	7
5	GAZER imaging options	10
6	The Utah State University mobile observatory facility that housed GAZER during the SPIRIT campaign	14
7	The Optical Pointing System mounting head with a USU radiometer installed	19
8	A photograph of the Optical Pointing System control console	20
9	A photograph of a single video frame from an extremely sensitive video camera, showing OH structure	22

LIST OF TABLES

<u>Table No.</u>		<u>Page</u>
1	GAZER Specifications	11
2	Optical Pointing System Specifications	17

INTRODUCTION

Utah State University (USU) was awarded a contract by AFOSR, Contract No. AFOSR-84-0192, based on a proposal "Infrared Airglow Clutter" submitted in response to the DOD-URIP FY84-85 Announcement. Proposed were two systems to augment an existing infrared (IR) experiment (i.e., an interferometer-spectrometer and a telescoped radiometer) at USU for systematic measurements of hydroxyl (OH) and molecular oxygen (O₂) IR airglow emissions, which are valid to the dynamics and photochemistry of the mesopause region. Specifically, the two proposed systems were:

- 1.) A low-light-level TV imaging system that is sensitive to OH-meinel emissions (6800-9000Å), and
- 2.) An optical positioning system for the IR radiometer. The TV imaging system, called GAZER, is required to provide images of the gross infrared band structures and wave motions generated by gravity waves. The microprocessor controlled tracking mount will drive a USU IR radiometer through programmable, repeatable scan patterns to provide sky maps of the temporal and spatial small scale inhomogeneities. These three systems (the existing interferometer-spectrometer, GAZER, and the scanning radiometer) would be incorporated into the Mobilab Auroral/Airglow Research Facility (MARF) at Utah State University. MARF contains supporting experiments/scanning photometers, all-sky TV, magnetometer, riometer, recording equipment, etc., for scientific investigations of spatial and temporal characteristics of IR emissions associated with the aurora and airglow. The two proposed instruments would provide the capability to make high resolution spatial and temporal measurements of IR structures. This is necessary to the establishment of the IR data base for study of the dynamic structuring and photochemistry of the mesopause region and will include the twilight transition for the photochemistry of OH and O₂, night airglow for information on dynamical processes, seasonal trends in emission levels and temperature identification of principal nightglow mechanisms.

APPROACH

The proposed approach was to procure a low-light-level OH video system and the optical pointing system from subcontractors through the competitive bid process. However, studies and investigation by USU showed that the program could be accomplished more effectively and the desired increased measurement capability could still be obtained within proposed costs if an alternate approach was taken, i.e., modification of existing equipment at USU to achieve the desired goals. The GAZER (Graphics Aided Zonal Energy Recorder), under development at USU for the Air Force Geophysics Laboratory for auroral measurements, would be modified, particularly in the front end, with a more sensitive TV camera and filter, etc., to be capable of airglow emissions measurements. The optical positioning system would be obtained by modifying an existing pedestal at USU by providing a programmable control unit, the motor drive system, and a data recording and analysis unit with the capability to control the instrument scan. With AFOSR approval, USU proceeded to develop these systems and both systems have been completed. GAZER was deployed to a remote site in the auroral zone in support of the AFGL SPIRIT program and operated successfully. The scanning radiometer is planned to support the AFOSR sponsored MAPSTAR investigation in September/October 1987. The following describes the GAZER and Scanning Radiometer systems.

GAZER

BACKGROUND

GAZER is a low light level, wide angle TV imaging and recording system designed for use in studies of atmospheric light emissions. Its main advantage over conventional low-light-level TV imaging and recording systems is that it has the capability of storing information regarding absolute intensity levels of the image for subsequent recall and analysis. GAZER has the capability of imaging signals ranging from the low light levels

associated with airglow, to the much brighter levels of intense aurora.

The system employs a filtered, image intensified, wide angle camera to obtain images which are then digitized (on an individual pixel basis) and stored on magnetic tape. Simultaneously, the images are displayed in false color to provide a visual indication of light emission intensity vs. position. Gazer is capable of some limited real time signal processing, but more complicated analysis requires the use of more powerful computers. The real time processing available however, makes a vast amount of information readily accessible to the user, thus enabling more effective decisions regarding approaches and procedures for further data acquisition.

One major application of GAZER will be in the determination of ionizing particle energy spectra from observed auroral emission rates. In particular, study of the ratios of the commonly observed emissions of 6300A and 5577A from atomic oxygen and the 4278A band from ionized molecular nitrogen should infer a characteristic energy of the electron flux that produced the emissions. A paper (Rees and Luckey, 1974) dealing with this technique is included with this report as Appendix A.

System Description

The GAZER system is shown in conceptual block diagram form in Figure 1. Figure 2 elaborates on the GAZER camera head. Figure 3 is a photograph of the instrument console and Figure 4 is a photograph of the Remote Camera Controller and the TV camera. Although the photographs shown in Figures 3 and 4 do not show GAZER installed in the USU mobile observatory, the instrument can be removed from the instrument cabinets shown and be installed into the mobile facility. As shown, the instrument is prepared for use in the laboratory or at remote sites where it is not feasible to utilize the mobile unit.

Operator control of the GAZER system is accomplished from the Televideo Control Terminal. This station displays the operational status of GAZER, and affords the operator programming



Figure 3. A photograph of the GAZER instrument console.

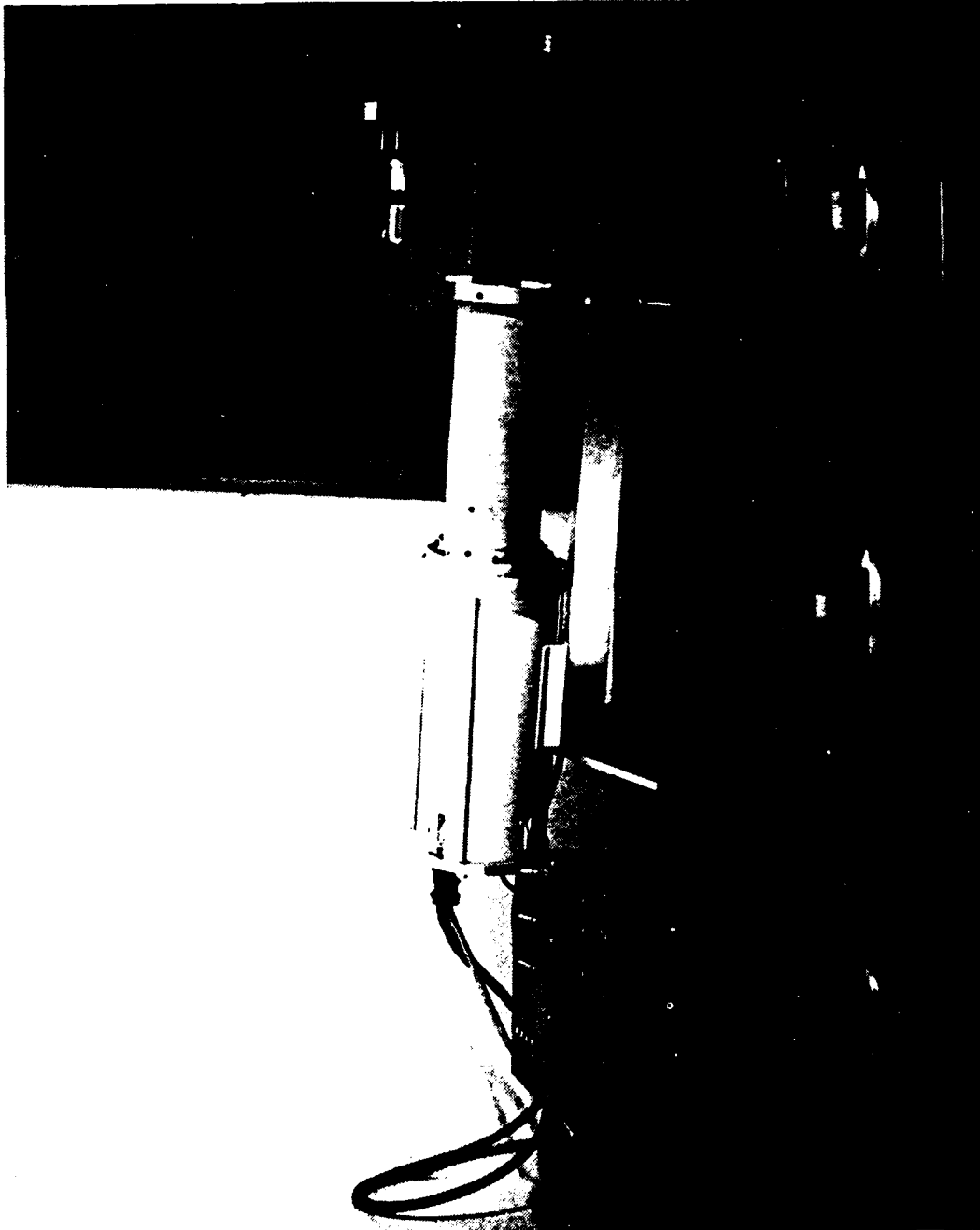


Figure 4. A photograph of the GAZER remote camera controller and the TV camera. The photograph also shows a new filter wheel and telecentric lens that were added to the front end of the camera subsequent to the work reported herein.

options and mode-of-operation selection. From the control terminal the operator monitors the status of power and temperatures, views and selects variable gains and sample rates, selects filters and controls the video displays. GAZER is capable of operation in any of 4 modes. These modes are user defined and can be preprogrammed to fit specific needs. A fifth mode is available for playback of recorded data and is not programmable. In each of the user-defined modes, such items as filters, gain, frame averaging/integration, frame rate and display aspects are programmed into a 10-command sequence. Thus, each mode can be tailor made for specific observing conditions.

Commands from the control console keyboard are sent to the system CPU which issues the system commands. The CPU is an 8086 device utilizing multi-bus I architecture. As can be seen from the diagram in Figure 1, the CPU interfaces with the Remote Camera Control over an RS232C Serial Control/Data bus.

The Remote Camera Control unit provides the interface with the GAZER camera head. It communicates video gain, intensifier gain, and filter position to the Camera Head, and monitors these parameters as well as preamp video.

GAZER is equipped with a Lenzar wide angle, low-light-level TV camera that incorporates a built-in image intensifier and a 6 position filter wheel. The Camera Head is shown in Figure 2. Filters incorporated in the system are described in the GAZER specifications shown in Table 1. Filter wheel position, and both the video camera gain and the image intensifier gain can be independently controlled. This produces a wide dynamic range capability for the system. In addition to receiving operational commands, the TV camera/intensifier incorporates monitors for temperature and voltage levels within the unit. As stated above, all control and monitoring functions for the Camera/Intensifier are accomplished from the GAZER Remote Camera Controller.

Video output from the intensifier/camera is sent to a color video monitor and then is converted from NTSC to digitized (8 bits per pixel grey scale) RGB (Red, Green, Blue) video for storage on magnetic tape and monitoring on the RGB color monitor.

Each frame recorded on the tape is preceded by a header that defines the system settings that were used to obtain the image. Conversion of the NTSC video to digitized video is accomplished by Imaging Technology Frame Grabbers. The image viewed here by an operator is color enhanced (false color) and directly shows intensity of light from the night sky. After it passes through the RGB monitor, the video signal is converted back to the NTSC format and is made available for monitoring and storage on the VHS recorder. The VHS recorder is maintained as a "log" of activities, while the tape mass storage unit serves as the "science" record.

Several imaging options are available for selection by an operator of GAZER. Figure 5 depicts these options.

If the operator selects the multiple image option, four separate images are displayed on the monitor, each being updated as the instrument continues to acquire data. Three of the images in this format correspond to the three filtered images. The fourth image can be a composite of these images or can display the red-blue ratio. Each image includes information on filter, time and date of the image.

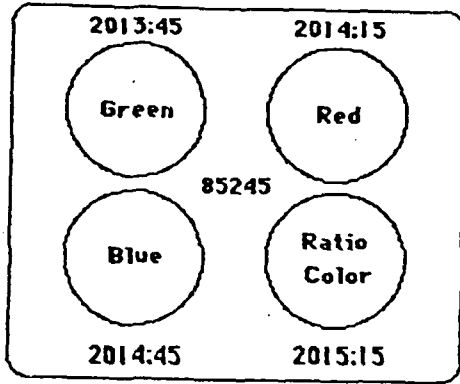
The second imaging option shows a single image. The image to be displayed and its frequency of update is under user control. The user is able to select the wavelength of the image to be viewed (red, green, blue, or composite). Also displayed is the filter involved, time and date of the image.

With the Scan option the operator can select a diagonal across the image (any direction) along which the brightness can be displayed in bar chart form below the image. This essentially provides a meridian scan to monitor development of auroral activity or other phenomena. Filter information and time and date of the image are also displayed.

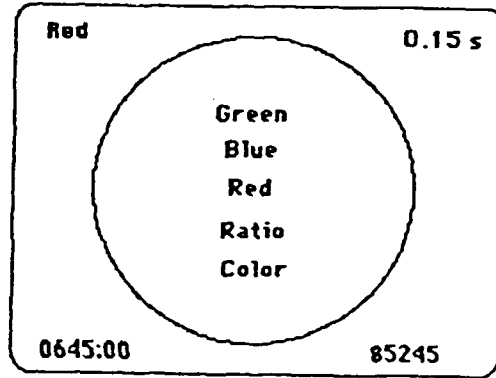
If the user selects the Magnified option, two images are displayed, one of the entire field-of-view and the other of a magnified portion of that field. A "window" defining the area to be magnified appears in the unmagnified view. The window size is adjustable and position is variable, thus allowing the operator

USU

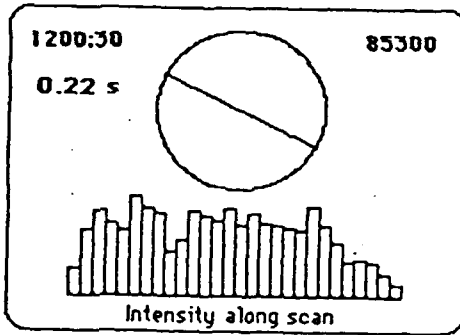
GAZER IMAGING MODES



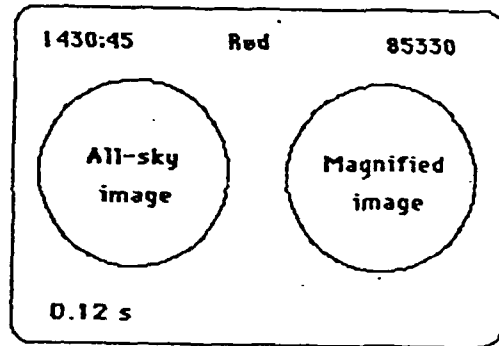
Multiple Image Mode



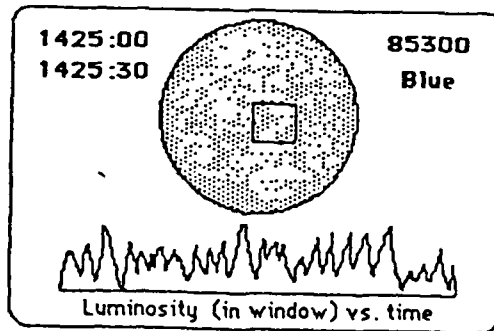
Single Image Mode



Scan Mode



Zoom Mode



Pulsation Mode

FTB
13-Mar-85

Figure 5. GAZER imaging options.

to "zoom" in on a region of the field that is of interest.

The final option is designed to allow the recording of a brightness history of a selected part of the image. A small adjustable window is positioned within the field-of-view, and the system produces a plot of the luminosity within the window vs. time. With this option the measurements are restricted to the use of a single filter. The plot is displayed beneath the image of the sky as shown in the Figure.

TABLE 1.
GAZER Specifications

Item	Specifications/Parameters
VIDEO SENSOR:	
Camera	LENZAR Intensicon-8 LLLTV using 2nd gen micro-channel intensifier and proprietary camera tube.
Sensitivity	Full video at 1×10^{-6} ft-c 3db points at 1×10^{-7} ft-c Usable information at 1×10^{-8} ft-c
Spectral Sensitivity	400 - 930nm
Resolution	400 lines at center at 1×10^{-6} ft-c 250 lines at center at 1×10^{-8} ft-c
Dynamic Range at a given gain (Gray Scale Rendition)	10 shades of gray using EIA TV resolution chart (to 1×10^{-6} ft-c)
Filter Wheel	6 positions Blue glass bp filter 356 - 450 nm at 0.707 transmission 334 - 480 nm at 0.200 transmission Green glass bp filter 492 - 550 nm at 0.707 transmission 466 - 588 nm at 0.200 transmission Red glass lp filter 614 nm at 0.707 transmission 602 nm at 0.200 transmission Neutral density filter (0) Neutral density filter (1) Neutral density filter (5)

Table 1 (Cont.)
GAZER Specifications

Item	Specifications/Parameters
Lenses	16 mm format, C-mount 12.5 mm f/1.3, FOV 65° diag., 54° x 42° 4 mm f/1.8, FOV 126° diag., 115° x 100°
Gain Control . . .	Intensifier - External analog program voltage, 1000:1 range Video Chain - External analog program voltage, 1000:1 range
Physical Mounting .	Contained in environmentally controlled case with custom mounting
VIDEO PROCESSOR	
Central Processing Unit	8086 CPU, Multi-bus I architecture
Frame Grabber . . .	3 frame buffers, 256K bytes per buffer, 2 interlaced fields per buffer
Resolution	512 x 512 pixels, 8 bits per pixel gray scale
Color	Artificially added on basis of gray scale to conform to landsat standards
Processing Rate . . .	10 seconds per frame, including display computations and mass storage for single frame, 20 seconds for BRIM computations and storage
Processing Modes .	Color ratio (BRIM) single image; Multiple image including color ratio; Intensity along an arbitrary cut; Magnified image; Luminosity in a window vs. time.
Mass Storage	Quarter-inch magnetic tape cartridge, 67 Mbytes per cartridge
Display	RGB color; NTSC encoded composite color video
Log	VHS cassette video recorder.

GAZER Field Operations

GAZER was deployed at Fort Nelson, British Columbia in support of the AFGL SPIRIT campaign from January to April 1986. During that interval more than 1500 megabytes of data were acquired including observations during the February 9, 1986 magnetic storm, one of the largest of the decade. During the evening of the SPIRIT rocket launch, GAZER acquired four images per minute over a two-hour interval centered on the time of launch, for a total of approximately 450 images. The data recorded during the launch represent roughly 8% of the total data acquired over the course of the campaign. Figure 6 shows the USU mobile facility that housed GAZER during the SPIRIT campaign.

At the time of the SPIRIT campaign GAZER was configured as herein reported, i.e., with an internal filter wheel (within the camera housing) and a wide angle C-mount lens as the primary camera lens but was installed in the mobile observatory rather than in the rack mount shown in Figure 3. This configuration imposed certain constraints on the system, the most severe being that monochromatic interference filters could not be used in the optical chain. Instead of interference filters, red, blue, and green glass filters, selected to pass certain dominant features of the auroral spectrum, were installed. Three neutral density filters were also installed, providing neutral densities of 0, 1, and 5. The blue, green and red glass filters had peak responses near 3950 Å, 5200 Å, and >6100 Å, respectively, and had half peak bandwidths on the order of 100 Å. Hence, the blue glass filter passed both the 3914 Å and 4278 Å auroral band emissions, while the green filter was dominated by the 5577 Å emission. The red filter passed only wavelengths longer than 6100 Å and was therefore primarily responsive to the 6300 Å emission.

As mentioned earlier, the operating mode of GAZER is under operator control. That is to say, the filter sequence, integration time and console display can be configured to suit the particular conditions. Also, the operating modes can be predefined and recalled for use by the operator. During the



Figure 6. The Utah State University mobile observing facility that housed GAZER during the SPIRIT campaign.

SPIRIT campaign several operating modes were predefined, each mode was designed to acquire data under specific auroral conditions. All, of these modes were tested during the SPIRIT field campaign. During the SPIRIT launch, GAZER was configured to cycle between the blue and red filters at intervals of approximately 15 seconds (time between images is a function of the time required to store an image to magnetic tape). In the 'patrol' mode (i.e., without data storage) the cycle time is reduced to approximately 5 seconds between frames.

The digital data acquired by the GAZER system opens up a vast new spectrum of data analysis opportunities. The images can be corrected for lens distortion, filter characteristics and van Rhijn effects and the auroral forms can be mapped into geographic or geomagnetic coordinate systems. A variety of image processing techniques, such as bandpass filtering, background removal, temporal integration over multiple frames or spectral ratioing can be readily performed. Although monochromatic filters were not incorporated in the GAZER system at the time of the SPIRIT launch, we feel that the data in hand will allow us to derive a first order approximation of the auroral energy deposition by utilizing the images acquired using the blue and red filters. We propose to derive the ratio of the red to blue intensity over small spatial regions within the aurora and to examine how that ratio varies within individual images and as a function of time during the auroral substorm.

Work by *Rees and Luckey* [1974] has shown that the spectral energy distribution of auroral electrons in the energy range 100 eV to 10's of keV can be expressed in the form

$$N(E)dE = N_0 E \exp(-E/\delta) dE$$

where E is the energy at the peak of the distribution. Using the theoretical curve published by *Rees and Luckey*, δ can be expressed as follows:

$$\delta = 2.014/R$$

where R is the ratio 6300Å/4278Å.

There are some obvious limitations to the data acquired by GAZER in that the filters were not monochromatic and the images were not acquired simultaneously at both wavelengths. However, the quality of the data is high and the software tools developed in processing these data will be of value in future campaigns. It is of note that in the time period subsequent to the SPIRIT measurements campaign some further modifications have been accomplished to the GAZER system. These include the installation of a wide angle telecentric lens and monochromatic filters in the optical chain.

THE OPTICAL POINTING SYSTEM

The Optical Pointing System consists of three main components: 1.) the rotatable instrument mount, 2.) the control unit, and 3.) a PDP 11/73 computer. Figures 7 and 8 show the rotatable instrument mount housing a USU IR radiometer, and the pointing system controller, respectively. Specifications for the optical pointing system are shown in Table 2.

TABLE 2.
Optical Pointing System Specifications

Parameter	Specifications/Comments
Tracker Modes:	
Elevation Scan	Tracker scans continuously through an elevation range, then steps discretely in azimuth and retraces through the elevation range.
Azimuth Scan	Tracker scans continuously through an azimuth range, then steps discretely in elevation and retraces through the azimuth range.
Manual Positioning	Manually move the tracker to any position using keys on the front panel of the control module.
Scan Parameters:	
Elevation Scan	Start angle - set manually (0.0° to 359.9°). Scan Range - 180°, 90°, 60°, 45°, 30°, or 15° rotation. Scan Direction - ± (CW or CCW). Scan rate - 0.2 to 2.0° per second. Azimuth step size - 1°, 2°, 4°, or 8°.
Azimuth Scan	Start angle - set manually (0.0° to 359.9°). Scan range - 360°, 180°, 90°, 60°, 45°, 30°, or 15° rotation. Scan direction - ± (CW or CCW). Scan rate - 0.2 to 2.0° per second.

TABLE 2 (Continued).
Optical Pointing System Specifications

Parameter	Specifications/Comments
Azimuth Scan (cont.) . .	Elevation step size - 1°, 2°, 4°, or 8°. Elevation step range - 0°, 16°, 32°, or 48°.
 Outputs:	
Elevation Position . . .	Four digits, seven segment LED readout. Digital stream; synchronous serial output at 1200 baud for recording on tape.
Azimuth Position	Four digits, seven segment LED readout. Digital stream; synchronous serial output at 1200 baud for recording on tape.

The Optical Pointing System Control Unit provides control of the instrument mount through two cables. One cable is utilized to drive the motors on the tracker while the other cable is utilized for position feedback provided by optical encoders on the tracking mount. The data from the dual channel radiometer and the position and the position data are recorded simultaneously and post-processed. The PDP-11/73 is part of the total system that is used to process the data at the operating field site. The PDP-11 has the capability to control the instrument scan through various regions of the sky during any set measurement period. The control unit is also supplied with a serial interface to allow communication with the host computer. This unit is thus programmable to allow any type of spatial scan to be used.

A photograph of a single video frame from an extremely sensitive video camera operating in the 7100-8000A is shown in Figure 9. The photograph clearly shows OH structure and stars visible in the background.

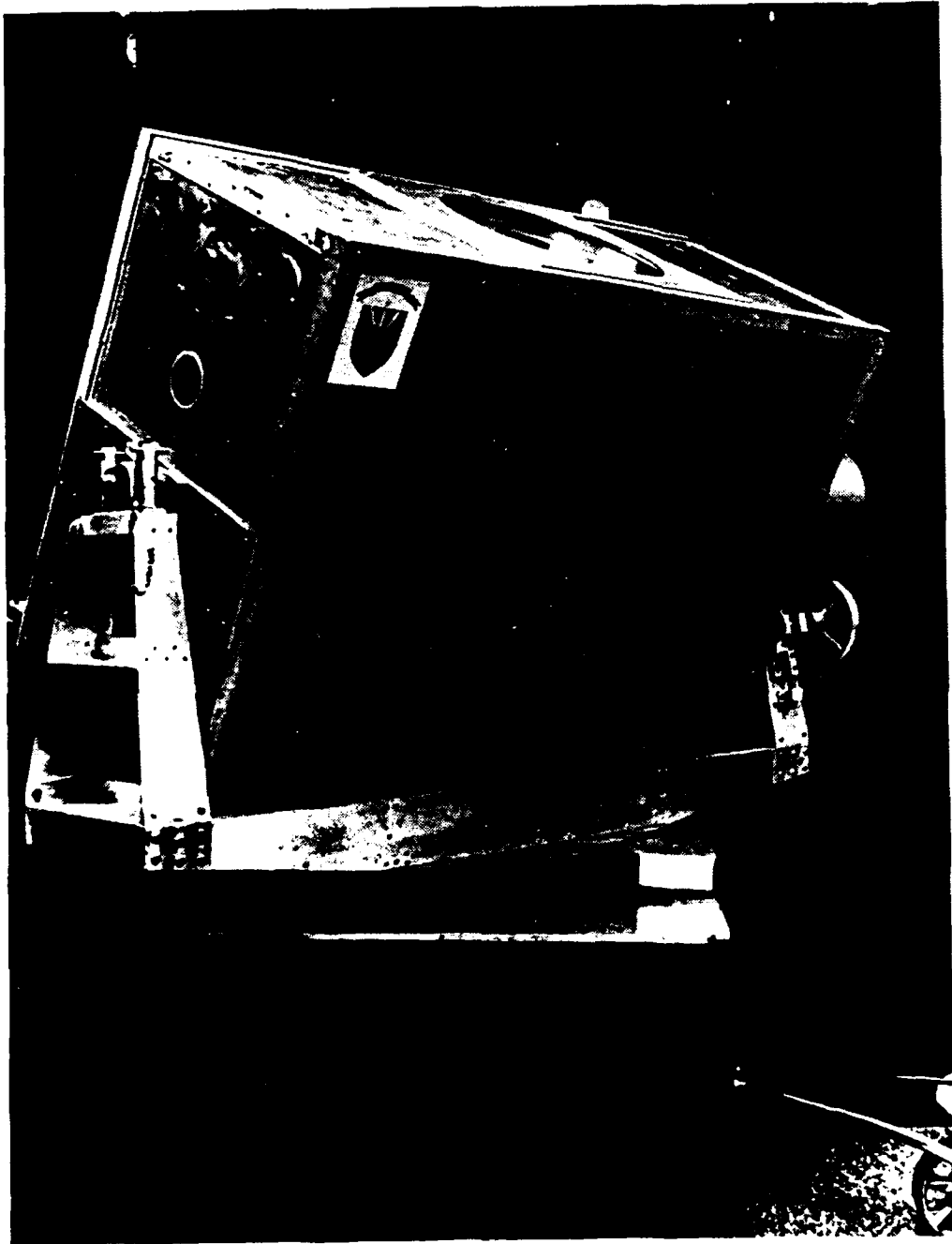


Figure 7. The Optical Pointing System mounting head with a USU radiometer installed.

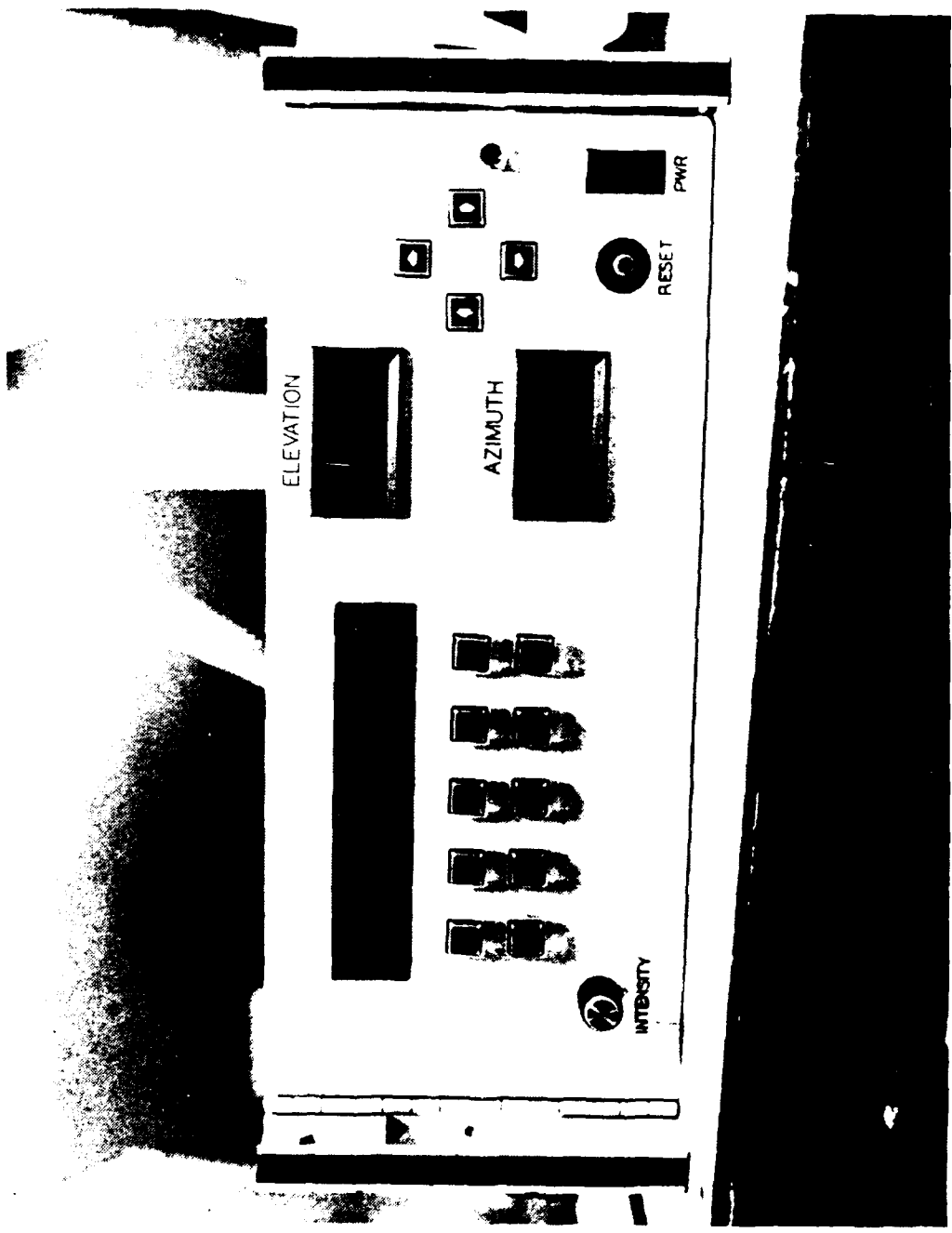


Figure 8. A photograph of the Optical Pointing System control console.

When the video frame shown in Figure 9 was recorded, the USU interferometer was coaligned with the camera and the center of its field-of-view is marked with an "X". The interferometer field-of-view is approximately 1.8 cm in diameter on the photograph. The interferometer is measuring a "dark" band in the frame. Field-of-view of the photograph is $9^{\circ} \times 12^{\circ}$. The "dot" indicates the center of the fixed radiometer field-of-view. With the scanning radiometer this type of structure will be mapped and recorded continuously to give a capability to investigate the spatial and temporal characteristics of structure of the airglow.

The scanning radiometer is planned to support the AFOSR sponsored MAPSTAR investigation in September/October 1987.



Figure 9. A photograph of a single video frame from an extremely sensitive video camera showing OH structure.

APPENDIX A

Auroral Electron Energy Derived From Ratio of Spectroscopic Emissions

1. Model Computations

M. H. REES¹

National Science Foundation, Washington, D. C. 20550

D. LUCKEY

*Laboratory for Atmospheric and Space Physics, University of Colorado
Boulder, Colorado 80302*

The relationship between auroral electron fluxes and spectroscopic emission features in aurora is quantitatively explored. The model computations focus on the prominent auroral radiations of atomic oxygen at 6300 Å and 5577 Å and a vibrational band of ionized molecular nitrogen at 4278 Å. The emission rate ratios, 6300/4278, 5577/4278, and 6300/5577, together with the absolute emission rate of the 4278-Å radiation, may be used to infer a characteristic energy of the precipitating electron flux. This characteristic energy and the 4278-Å intensity then determine the total electron flux and the energy deposition rate. Computational results are presented in easily used curves, and the assumptions made in the model calculations are discussed in the text. At the present time it appears that the ratio 6300/4278 is the most reliable and informative of the set.

Numerous in situ measurements of auroral electron fluxes have been made from rockets and satellites since the first detector was flown into an auroral display in 1958 [Mellwain, 1960; Meredith *et al.*, 1958]. Likewise, auroral spectroscopy has been carried out for over a century, since the early work of Angström [1869]. Only in recent years, however, have the physical processes that relate electron bombardment to spectroscopic emissions been understood sufficiently well to allow detailed computations on this problem. The monograph by Chamberlain [1961] provides most of the fundamental concepts required to model the spectroscopic aurora, and Omholt's [1971] concise book updates some details in formulation as well as many numerical parameters.

Spectroscopic emissions in the wavelength region accessible to ground-based observations account for only about 4% of the energy deposited in the atmosphere by auroral bombardment (M. H. Rees, manuscript in preparation, 1974). The power of spectroscopic measurements lies in the fact that they provide a surprisingly large amount of information about the energy deposition rate, the number flux, and the characteristic energy of the bombarding electrons (and protons). However, spectroscopic measurements give little information about the angular distribution of electron streams and rather limited information about the angular distribution of the protons.

Jones and Rees [1973] and Rees and Jones [1973] have shown that the spectroscopic morphology of auroral radiations depends on the time history of the precipitation; each of the several processes that contribute to the production of excitation resulting in observable optical emissions has its own characteristic time constant. Variability in the ratios of various spectroscopic features can be expected solely because of the temporal variations in the magnitude of a particle flux of constant energy characteristics. However, the largest changes in the ratios of certain spectroscopic emission features are caused by the wide range of energy spectra that characterize auroral electron precipitation, the energy dissipation properties of the at-

mosphere, and the changes in the composition of the neutral atmosphere with altitude. Electrons of different energies are stopped at different heights; they excite atoms and molecules in proportion to the abundance of each species at that altitude. Nonlocal excitation may be important if secondary electrons undergo transport before dissipating their energy or if a large flux of ultraviolet photons capable of ionizing and exciting gases is produced. In addition, some metastable species are collisionally quenched before a radiative transition occurs; the rate of quenching depends on the abundance of the quenching species.

In this paper we investigate the effects of various electron energy spectra on the photon emission rates of three auroral radiations, the 6300-Å and 5577-Å lines of atomic oxygen and the 4278-Å band of ionized molecular nitrogen. In particular, we wish to learn if it is possible to use ratios of these commonly observed auroral spectroscopic features to infer a characteristic energy of the electron flux producing the emissions. Eather and Mende [1972] and Gattinger and Vallance Jones [1972] obtained ratios of spectroscopic emissions from measurements made during a series of airplane flights in various portions of the auroral oval. Using these observations, Eather and Mende [1972] were able to identify regions of soft electron precipitation in the polar cleft and the auroral oval. Their conclusions were based on preliminary results of the computations reported here.

Judge [1972] carried out simplified model computations directed toward essentially the same goal as ours. Although Judge takes into account the fact that spectroscopic ratios are a function of the electron energy, he does not include the dependence of the ratios on the flux magnitude, i.e., the absolute intensity of the emission features. The effect of the absolute intensity on the ratios appears to be significant, indicating the importance of excitation processes other than electron impact, processes that Judge [1972] has neglected.

MODEL COMPUTATIONS

The physical processes that relate electron bombardment of the atmosphere to optical radiations are illustrated schematically in Figure 1. Primary electrons cause ionization,

¹On leave from the University of Colorado, Boulder, Colorado.
Copyright © 1974 by the American Geophysical Union.

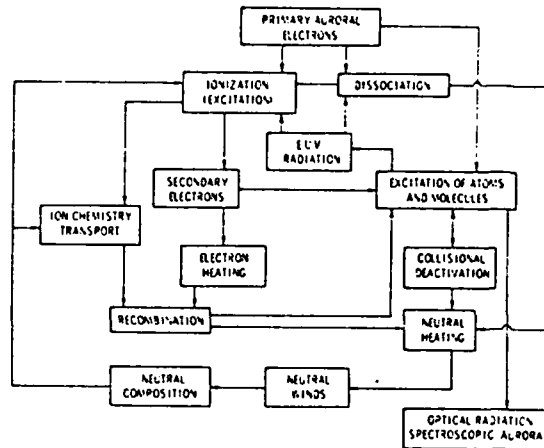


Fig. 1. Schematic flow chart relating auroral electron fluxes and optical emissions.

dissociation, and dissociative ionization, many ions and atoms being produced in excited states. Some of these excited states will radiate ultraviolet photons with sufficient energy to produce further ionization, etc. We do not need to consider this source of ionization separately, since it is already included in the experimental value for the amount of energy lost per ion pair formed, about 35 eV. Similarly, we need not explicitly distinguish between primary, secondary, tertiary, etc., electrons that produce the ion pairs. Chemical-ionic reactions convert the ion species produced initially into different ion species by charge exchange and ion-atom interchange. The chemical processes that are included in our model have been described by Jones and Rees [1973] and Rees and Jones [1973]. In general, atomic ions are converted into molecular ions that eventually undergo dissociative recombination. Our model includes two major sources of atomic and molecular excitation, energetic electron impact and dissociative recombination. It also includes thermal electron excitation of the $O(^1D)$ state. Electron impact dissociative excitation and dissociative excitation by EUV photons (E. C. Zipf, manuscript in preparation, 1974) have not been included. Although both processes are energetically capable of $O(^1S)$ excitation (as well as $O(^1D)$ excitation), the relevant cross sections are unknown at this time. The various excitation processes are described in detail by Rees and Jones [1973]; they will not be repeated here. The above reference also gives the reasons for not including certain reactions. In this model we have assumed that all secondary, etc., electrons dissipate their energy locally. This represents a very good approximation below 200 km; however, at higher altitudes, upward transport becomes increasingly more important [Banks et al., 1974], leading to nonlocal excitation.

A fraction of the electron energy goes into heating the ambient electron gas, thus raising the electron temperature. Rate coefficients for dissociative recombination depend on this electron temperature. Although we have not coupled the ion chemistry and electron and ion temperature computations, we have used temperature profiles appropriate to each model. If quenching reactions are included in the calculation, as much as one half of the energy input by auroral electrons goes into kinetic energy of the neutral gas. The consequences of neutral heating have been explored by Hays et al. [1973] and Volland and Mayr [1971]. These studies indicate that substantial changes in neutral composition can occur. Since even the un-

perturbed composition is uncertain, especially in the auroral regions, we have not attempted to include these changes in composition in the model.

Primary auroral electron fluxes have a wide range of energy distributions, including nearly monoenergetic components. An interesting problem is posed by the nature of the particle acceleration mechanism(s) that can produce the variety of the energy distributions that have been observed. Since an investigation of this problem requires detailed knowledge of the energy spectrum as well as the angular distribution of the energetic particles, the present study cannot shed any light on this question. We use spectroscopic observations to determine both the rate of energy deposition by auroral electrons and a characteristic energy that describes the electron flux. The choice of a 'typical' spectrum must be somewhat arbitrary. A frequently observed spectral energy distribution of primary auroral electrons in the range of 100 eV to some tens of keV has a Maxwellian form:

$$N(E) dE = N_0 E \exp(-E/\alpha) dE \quad \text{el cm}^{-2} \text{ s}^{-1} \text{ eV}^{-1} \quad (1)$$

where α is the energy at the peak of the distribution. The total number flux for such a distribution is $F = N_0 \alpha^2$, and the energy flux is $\xi = 2\alpha F$. The distribution described by (1) approaches zero for both small and large values of energy E , and thus the need for arbitrary cutoffs is eliminated. The large electron fluxes that are predicted below 100 eV consist almost entirely of secondary electrons [Rees and Maeda, 1973]. Substantial overlap in the energies of the primary and secondary electrons exists around 100 eV. Judge [1972] chose a double Maxwellian distribution to represent the electron energy distribution. Typical observed composite spectra [cf. Frank and Ackerson, 1971; Ogilvie, 1968] show that the energy distribution of the low-energy secondary electrons is more closely described by a power law.

Following the scheme illustrated in Figure 1, we have made sets of model computations for electron fluxes of different characteristic energies over a range of magnitudes. The reader is referred to previous papers [Rees and Jones, 1973, and papers cited therein] for the computational details. Figure 1 shows that several measurable parameters emerge from the model computations: electron and ion densities and temperatures, secondary electron fluxes, and many optical radiations. Here we will consider only three spectral features, the $N_2^+ \text{ I NG}(0, 1)$ band at 4278 Å, an allowed transition, and the 'forbidden' $O \text{ I}$ transitions at 5577 Å and 6300 Å. The oxygen green line at 5577 Å is emitted by $O(^1S)$ atoms, which have a radiative lifetime of about 1 s and suffer collisional deactivation by ground state atomic oxygen. This upper excited state, $O(^1S)$, is produced by low-energy secondary electron impact, dissociative recombination, and other processes for which the cross sections are still unknown. The red lines, 6300, 6364 Å, originate from the $O(^1D)$ state, which is only 2 eV above the ground state of the atom. Secondary electron impact, dissociative recombination of O_2^+ , cascading from $O(^1S)$, and impact excitation by ambient electrons in the high-energy tail of the thermal distribution are believed to be the major sources of excitation for this level. The $O(^1D)$ is metastable, with a radiative lifetime of about 100 s. Rapid collisional deactivation by N_2 accounts for the fact that practically no radiation is emitted below about 180 km. This emphasizes the importance of the relative abundances of O and N_2 with respect to altitude. Therefore the neutral atmosphere is a crucial input to a model that relates electron energy to spectroscopic ratios. The neutral

atmosphere that we used in the computations is given in Jones and Rees [1973].

An investigation by Rees and Jones [1973] showed that the effects of temporal variations of the precipitating fluxes on optical radiations are significant. Forced to make an arbitrary decision regarding the duration of the event, we chose 1200 s for our calculations. In a precipitation event that remains unchanged for this period of time the emission rate of most spectroscopic features will approach a steady state value.

NUMERICAL RESULTS

Several values for the characteristic energy α of the electron energy distribution were used in the model computations: $\alpha = 0.3, 0.6, 1.6, 4.0,$ and 10.0 keV. For each value of characteristic energy, calculations were made for a range of electron flux magnitudes. These magnitudes were chosen so that the corresponding 4278-Å column emission rate would be in the range from about 100 R to several kilorayleighs, magnitudes that are associated with commonly observed auroras.

Altitude profiles of 6300/4278, 5577/4278, and 6300/5577 volume emission rate ratios are shown in Figure 2 for energy spectra characterized by $\alpha = 0.3, 0.6, 1.6, 4.0,$ and 10.0 keV. The 6300/4278 ratio curves for different α overlap up to about 160 km. The separation of the curves above this point is explained by the relatively smaller energy deposition at high altitudes associated with the more energetic spectra. This results in lower electron densities at high altitudes; thus less of the energy available for excitation of the O(¹D) state is lost to electrons in this case than in the case of softer electron spectra. The separation of the 5577/4278 curves below 120 km is caused by an increase in the dissociative recombination source for the O I ($\lambda 5577$) emission due to the additional ionization and excitation produced by the more energetic spectra at low altitudes. The general shape of the ratio versus altitude curves is a result of the relative abundance of O and N₂ and the

collisional deactivation that affects O(¹S) below about 120 km and O(¹D) below about 250 km. Except for the minor departures described above, we note that altitude profiles of volume emission rate ratios are independent of the electron energy spectrum. Therefore such profiles would not be useful in determining energy characteristics of the bombarding flux. These ratios could suggest the relative abundances of the neutral species O, O₂, and N₂; however, additional computations would be required to assess this effect. The altitude profile of the 5577/4278 ratio is nearly constant above 160 km, and thus a conclusion reached earlier by Dalgarno and Khare [1967] is confirmed.

Optical measurements of auroral radiation can provide only column-integrated emission rates for both ground-based observations and satellite and rocket measurements. Often the assumptions used to derive altitude profiles from these measurements cannot be fully justified. Thus it is advantageous for the model to deal directly with measured column emission rates, using only well-defined assumptions. We assumed that the electron precipitation is field aligned, choosing a dip angle of 77° for these computations. We also assumed that the horizontal extent of the precipitation is sufficiently broad to fill completely the field of view of a photometric detector looking upward along the field line.

Column emission rate ratios of 6300/4278, 5577/4278, and 6300/5577 are shown as functions of the 4278-Å emission rate in Figures 3, 4, and 5 for several values of α . The curves show that column emission rate ratios are a function of the magnitude of the flux, a result that previously was not recognized. The emission rate ratio 6300/4278 decreases with increasing excitation of $\lambda 4278$ because the electron impact excitation of O(¹D) must compete with elastic scattering by ambient electrons, vibrational excitation of N₂, etc., for the available secondary electron energy. At high altitudes, where low-energy electrons deposit their energy, electron heating becomes the dominant mechanism. The high 4278-Å emission rate implies large electron fluxes and high electron densities.

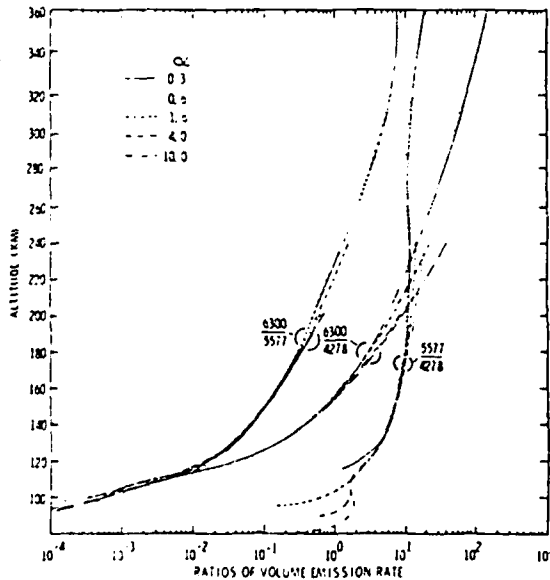


Fig. 2. Altitude profiles of volume emission rate ratios of 6300/4278, 5577/4278, and 6300/5577 for electron fluxes of different characteristic energies α . The energy input rate associated with the bombarding flux is $10 \text{ ergs cm}^{-2} \text{ s}^{-1}$ for the case of $\alpha = 0.3$ keV and $25 \text{ ergs cm}^{-2} \text{ s}^{-1}$ for the other three cases.

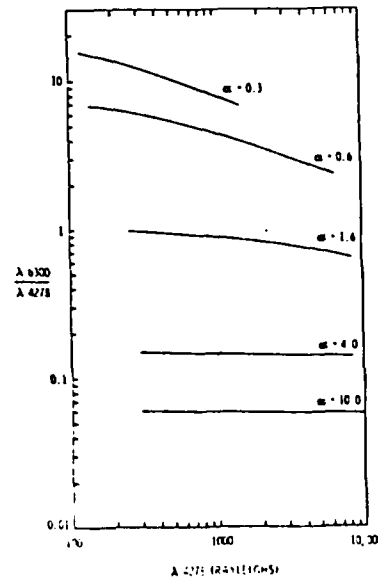


Fig. 3. Column emission rate ratio 6300/4278 as a function of the absolute emission rate of 4278 Å for electron fluxes of different characteristic energies α .

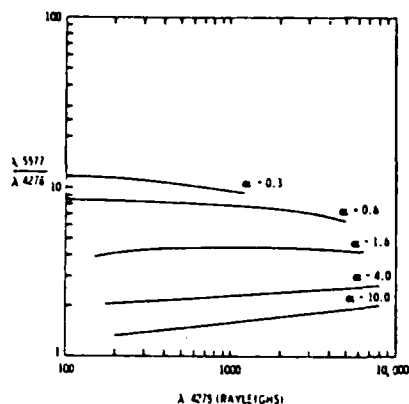


Fig. 4. Column emission rate ratio 5577/4278 as a function of the absolute emission rate of 4278 Å for electron fluxes of different characteristic energies α .

The resulting high degree of ionization leads to the channeling of more energy into the electron gas. Contributions to the 6300-Å emission from recombination and thermal excitation increase with increasing flux magnitude; however, these are minor sources of excitation in comparison with electron impact [cf. Rees and Jones, 1973]. At lower altitudes, vibrational excitation of N_2 and O_3 becomes the principal competitor for the energy. Electrons associated with harder electron spectra penetrate deeper into the atmosphere to levels where the molecular species are more abundant than atomic oxygen, this penetration explaining the decrease in the 6300/4278 ratio with increasing α .

The 5577/4278 ratio curves also show a variation with flux magnitude. Hard spectra ($\alpha = 10$) produce excitation at an altitude where the contribution to $O(^1S)$ excitation from recombination is significant. At this level the electron density varies as the square root of the ionization rate, which is approximately proportional to the 4278-Å emission rate. Thus an increase in ionizing flux results in increased recombination and increased 5577-Å emission, but the change is not linear. Since the excitation of $O(^1S)$ by soft primary electrons ($\alpha = 0.3$) is

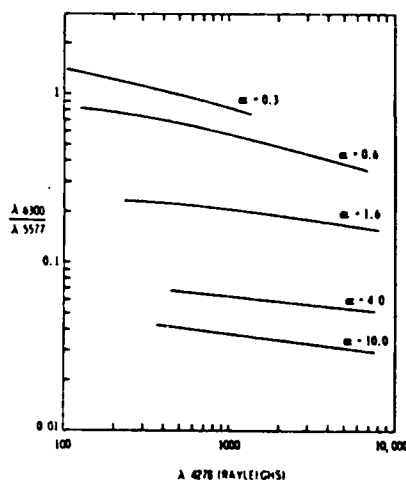


Fig. 5. Column emission rate ratio 6300/5577 as a function of the absolute emission rate of 4278 Å for electron fluxes of different characteristic energies α .

produced primarily by secondary electron impact, the arguments given to explain the behavior of the 6300-4278 ratio versus $\lambda 4278$ curves apply here also. However, the decrease in the ratio 5577/4278 with increasing flux magnitude is not as large as that seen in the 6300/4278 case because the threshold for excitation of $O(^1S)$ is more than 2 eV higher than the $O(^1D)$ threshold and the processes competing for the secondary electron energy are not as effective above 4.12 eV.

From the photometric measurements of emission rate ratios presented in Figures 3, 4, and 5 and the absolute emission rate of 4278-Å radiation the characteristic energy of the electron flux can be determined. With this α the total particle flux (and energy flux) can be found by using Figure 6, which relates total particle flux to the 4278-Å emission rate.

The 4278-Å emission rate per unit energy deposition rate is a parameter that is frequently used in auroral analyses [cf. Deehr *et al.*, 1970]. Until now it has been assumed that this quantity is a constant. Figure 7 indicates that this parameter depends on the characteristic electron energy, reflecting the change in composition with altitude. Thus even a simple calculation of the energy deposition rate requires the energy characteristic of the incident electron flux.

DISCUSSION

The curves presented relate electron precipitation to three prominent emission features in the visible portion of the auroral spectrum. A characteristic energy α for the electron stream can be found by using the ratio of 6300-4278 and the absolute emission rate of 4278 Å. With this α the particle flux and the energy input rate into the atmosphere can be deduced. A Maxwellian distribution of electron energy has been used in the model computations presented here. If the spectrum is not Maxwellian in shape, as is assumed, the quantity α will no longer have a mathematical significance; however, it can still be considered an energy characteristic. We have not explored the effects of different electron spectra owing to the large amount of computing time required to model the necessary ranges in flux and energy. We have previously shown [Rees, 1963, 1969] that for different electron spectra the altitude profiles of energy deposition, or ionization, assume different shapes; it is reasonable to infer that the excitation rates of optical emissions will likewise be different. However, since height-integrated parameters are probably less sensitive to the

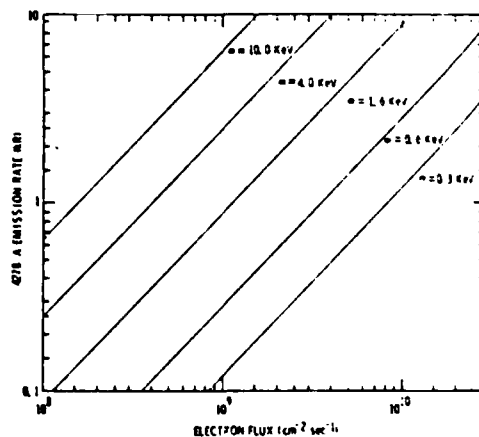


Fig. 6. Electron flux associated with a given emission rate of 4278-Å radiation for a range of characteristic energies α associated with the electron spectrum.

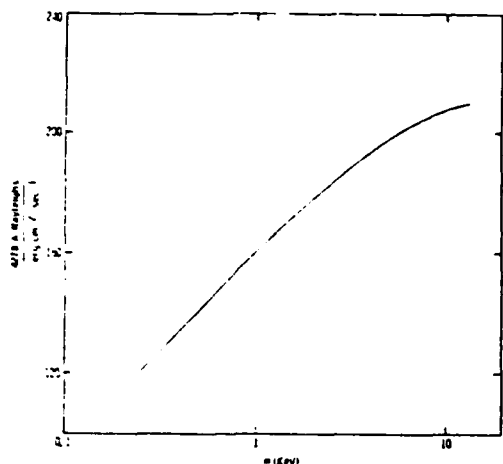


Fig. 7. Emission rate of 4278-Å radiation per unit energy deposition rate as a function of the characteristic energy α associated with the electron precipitation.

differences in detail in electron spectra, our model computations should generally be applicable.

Jones and Rees [1973] give a summary table showing that the observed ratio of molecular ions NO^+/O_2^+ varies considerably, and this large variability has since been noted by Swider *et al.* [1974], Narcisi *et al.* [1974], and W. E. Sharp (private communication, 1974). In general, the observed ratios are larger than those predicted by model computations that use accepted values for the rate coefficients and standard neutral atmospheric models. Nominal departures from the accepted input parameters produce only slight changes in the ratio NO^+/O_2^+ . It is possible to reproduce the large observed ratios by increasing the concentration of NO in the model; for example, a threefold increase in NO produces approximately a threefold increase in the ratio of the ions. Evidently, the ratio problem is coupled with the problem of enhanced NO abundance in the auroral ionosphere. Although these shortcomings in our auroral model must be recognized, they have only a small effect on the spectroscopic ratios under study. If the example above is used, a threefold increase in NO^+/O_2^+ changes the 5577:4278 ratio by 20% and has no effect on the 6300:4278 ratio.

There have been some observations of low-energy auroral electron spectra with characteristics that differ from those predicted by theory. Specifically, between about 20 eV and 60–85 eV the decrease in the electron flux can be represented by a power law $E^{-\gamma}$; theoretical calculations have determined γ to be between 2.2 and 2.4 [Rees and Jones, 1973; Banks *et al.*, 1974]. Observations by Sharp and Hays [1974] and Feldman *et al.* [1972] yield a value of 0.9 for the exponent γ in the power law for this energy range, whereas Ogilvie [1968] and Frank and Ackerson [1971] obtain an exponent of about 2.2. Unless an important energy loss process has been overlooked in the model computations, it may be necessary to consider the possibility that degraded primaries find their way to altitude levels lower than those allowed by energy considerations.

Fortunately, the cross sections for excitation of $\text{O}(^1D)$ and $\text{O}(^1S)$ peak below 20 eV, where the model and observations agree. Since both the electron flux and the excitation cross sections decrease with increasing energy, the product of the two quantities decreases rapidly; therefore electron energies

above 20 eV make only a small contribution to excitation of the metastable oxygen levels. The shape of the electron spectrum is not used to compute the 4278-Å emission. Thus although the electron spectral shape is an important issue, the effect it has on the spectroscopic ratios of the emission features presented here is only minor.

Ironically, the most prominent emission in the visible portion of the auroral spectrum, the 5577-Å radiation, is the most difficult to explain. Although electron impact and dissociative recombination are probably the most important sources of excitation, one cannot discount other mechanisms that may involve electron impact or photodissociation of O_2 , energy transfer reactions, or cascading from allowed levels of highly excited oxygen atoms. The 5577/4278 ratio curves must therefore reflect this uncertainty, as must the 6300:5577 curves. If consistent results are obtained by using the ratios presented here, confidence in our understanding of the 5577-Å excitation will increase.

The opportunity exists to test the validity of the spectroscopic ratio method of deducing electron energy spectra. The Isis 2 satellite carries particle detectors as well as photometric detectors on board, providing both input and output information for the model. The test event must be chosen carefully so that the aurora viewed by the photometer is, in fact, produced by the electron flux measured in situ [cf. Shepherd *et al.*, 1973]. Information from the instruments on board the Atmospheric Explorer satellites will also be valuable in this effort. Work along these lines is in progress.

Acknowledgment. The research has been supported by the Atmospheric Sciences Section of the National Science Foundation under grants GA 16290-1 and GA 40992.

The Editor thanks J. W. Chamberlain and E. C. Zipf for their assistance in evaluating this paper.

REFERENCES

- Angström, A., Spektrum des Nordlichts, *Ann. Phys. Leipzig*, **137**, 161, 1869.
- Banks, P. M., C. R. Chappell, and A. F. Nagy, A new model for the interaction of auroral electrons with the atmosphere: Spectral degradation, backscatter, optical emission, and ionization, *J. Geophys. Res.*, **79**, 1459, 1974.
- Chamberlain, J. W., *Physics of the Aurora and Airglow*, pp. 244–320, Academic, New York, 1961.
- Dalgarno, A., and S. P. Khare, The 5577/3914 ratio in auroras, *Planet. Space Sci.*, **15**, 938, 1967.
- Deehr, C. S., G. A. Gustafsson, A. Omholt, L. Anderson, A. Egeland, and H. Borg, Relation of low energy particle precipitation to the luminous aurora observed from Esro-1A, *Phys. Norv.*, **4**, 101, 1970.
- Eather, R. H., and S. B. Mende, Systematics in auroral energy spectra, *J. Geophys. Res.*, **77**, 660, 1972.
- Feldman, P. D., J. P. Doering, and F. A. Herrero, Auroral electrons and the optical emissions of nitrogen (abstract), *Eos Trans. AGU*, **53**, 1073, 1972.
- Frank, L. A., and K. L. Ackerson, Observations of charged particle precipitation in the auroral zone, *J. Geophys. Res.*, **76**, 3612, 1971.
- Gattinger, R. L., and A. Vallance Jones, The intensity ratios of auroral emission features, *Ann. Geophys.*, **28**, 91, 1972.
- Hays, P. B., R. A. Jones, and M. H. Rees, Auroral heating and the composition of the neutral atmosphere, *Planet. Space Sci.*, **21**, 559, 1973.
- Jones, R. A., and M. H. Rees, Time dependent studies of the aurora. I. Ion density and composition, *Planet. Space Sci.*, **21**, 537, 1973.
- Judge, R. J. R., Electron excitation and auroral emission parameters, *Planet. Space Sci.*, **20**, 2081, 1972.
- McIlwain, C., Direct measurement of particles producing visible aurora, *J. Geophys. Res.*, **65**, 2727, 1960.
- Meredith, L. H., L. R. Davis, J. P. Heppner, and O. E. Berg, Rocket auroral investigations, *IGY Rocket Rep., Ser. 1*, 169–178, 1958.

END

6-87

DTIC